Sensors and Materials, Vol. 38, No. 6 (2026) 2927–2940
MYU Tokyo

S & M 4478

Application of Carbon-fiber-reinforced Composite-packaged Fiber Bragg Grating Surface-bonded Sensors for Strain and Temperature Monitoring of Wind Turbine Blades

Yangrui Zhu,[1] Liangyang Luo,[1] Xiao Wang,[1]
Lin Wang,[1] Shuying Wang,[1] and Enlin Cai[1,2*]

[1]School of Electronic Information, Qingdao University, Laoshan District, Qingdao 266071, China
[2]Aerospace Information Technology University, Jinan 250200, China

(Received March 3, 2026; accepted April 21, 2026)

Keywords: carbon-fiber-reinforced composite, fiber Bragg grating sensor, wind turbine blade, strain and temperature monitoring, linearity

In this study, a carbon-fiber-reinforced composite packaged fiber Bragg grating (CFRP-FBG) surface-bonded sensor is developed for strain and temperature monitoring of wind turbine blades. To address the limitations of bare or simply bonded fiber Bragg grating (FBG)—such as insufficient mechanical protection, reduced strain-transfer efficiency, and poor operational stability—the proposed sensor uses a carbon-fiber-reinforced composite (CFRP) encapsulation structure that matches the blade substrate material, improving mechanical compatibility and strain transfer. Static cantilever-beam experiments show that the CFRP-FBG sensor exhibits a strain sensitivity of approximately 1.22 pm/με with a linearity of 0.9998, and the measured strain agrees with theoretical calculations and strain-gauge results within 1–2%, corresponding to a strain-transfer efficiency above 98%. Temperature calibration from −60 to 60 °C demonstrates a sensitivity of 18.63 pm/K and strong wavelength–temperature linearity. The sensor was further installed at four key positions on an operating wind turbine blade. Dynamic monitoring results indicate that the measured strain histories correspond closely to blade rotational speed and cyclic loading, without noticeable drift or signal loss during continuous operation. These results demonstrate that the CFRP-FBG sensor provides high sensitivity and feasibility for online strain and temperature monitoring of wind turbine blades under representative operating conditions.

1. Introduction

In recent years, with the rapid development of renewable energy technologies, the proportion of wind energy in the global energy mix has been steadily increasing. As a key component in wind energy conversion, wind turbine blades require structural health monitoring (SHM) to ensure operational safety and improve power generation efficiency.(1) Traditionally, resistance strain gauges (SGs) have been widely used for blade strain measurement; however, their long-term field application is often constrained by environmental influences, which may lead to drift

*Corresponding author: e-mail: caienlin@aitech.edu.cn
https://doi.org/10.18494/SAM6128

ISSN 0914-4935

or debonding failures and reduce measurement reliability. Conventional monitoring methods also struggle to simultaneously meet the requirements of real-time response and high accuracy. Meanwhile, carbon-fiber-reinforced composite (CFRP), owing to its excellent mechanical properties and lightweight characteristics, has gradually replaced traditional materials and become the preferred choice for wind turbine blades. Fiber Bragg grating (FBG) sensors, featuring high sensitivity, immunity to electromagnetic interference, and multiparameter measurement capabilities, have also shown great potential in SHM applications.[2]

Extensive research efforts have been carried out in both academia and industry to advance the engineering application of FBG sensors in SHM. Arsenault *et al*. developed a distributed strain-sensing system based on FBG, in which multiple gratings were deployed along the rotor and blade span.[3] Their laboratory static and dynamic loading experiments demonstrated the real-time acquisition of strain-field distributions and verified the feasibility of the system for load identification and SHM. Tian *et al*. attached twelve FBG sensors to the windward surface of a wind turbine blade and proposed a baseline-free damage identification method using static strain responses and chi-square statistics.[4] Their approach successfully located and quantified blade damage under various damage scenarios. Wen *et al*. embedded FBG sensors inside the three blades of a scaled floating wind turbine model and incorporated an optical rotary joint to construct an online blade load-monitoring system.[5] Real-time measurements of blade bending moments and torsional loads were obtained in wave-tank tests, demonstrating the reliability of FBG-based sensing in complex fluid–structure interaction environments. Pereira proposed a multistage SHM framework using FBG sensors during blade manufacturing, full-scale testing, and in-service monitoring.[6] The results showed that FBG can provide continuous strain and temperature information throughout the entire blade life cycle. Li *et al*. conducted a comprehensive review of blade damage-detection techniques and highlighted that strain-based monitoring using FBG or other optical fiber sensors can complement vibration- and acoustic-based methods, offering high sensitivity for early damage detection.[7] Wang *et al*. further summarized common damage modes in large composite blades and reviewed current strain-, vibration-, and acoustics-based monitoring approaches.[8] They emphasized that combining FBG sensing with multisource data fusion is a promising direction for achieving online SHM and lifetime prediction of large wind turbine blades.

Although significant progress has been made in FBG-based blade strain monitoring and damage identification—particularly in multipoint strain-field acquisition, load reconstruction, and detection of typical damage forms—most existing studies rely on bare FBG or simple surface-bonded configurations. In these cases, sensors still face challenges in mechanical protection, strain-transfer efficiency, as well as operational stability and durability under harsh field environments.[9] Moreover, systematic investigations into the compatibility between encapsulation materials and blade substrates, the combined strain–temperature performance, and long-term degradation mechanisms remain insufficient. To address these limitations, we propose and fabricate a carbon-fiber-reinforced composite packaged fiber Bragg grating (CFRP-FBG) surface-bonded sensor with a CFRP encapsulation layer matched to the blade substrate. The strain–temperature characteristics and monitoring feasibility of the developed sensor are evaluated through theoretical modeling, static loading tests, temperature calibration, and

monitoring on an operating wind turbine blade. Particular emphasis is placed on measurement accuracy, strain-transfer performance, and short-term operational stability. The present study is intended to verify the feasibility of the CFRP-FBG sensor for blade strain and temperature monitoring under representative service conditions, while further long-term investigations are still needed to assess creep-related effects, long-term drift, and its applicability to full structural health monitoring.

2. Materials and Methods

2.1 Principle of FBG sensing

FBGs are periodic refractive index modulation structures inscribed in the fiber core using ultraviolet light and are composed of the cladding, the grating region, and the optical fiber. When light of a specific wavelength (the Bragg wavelength) satisfies the Bragg condition, that wavelength is reflected while all other wavelengths continue to propagate through the fiber. The structural details are shown in Fig. 1.

The Bragg wavelength satisfies the relationship

$$\lambda_B = 2n_{eff}\Lambda\,, \tag{1}$$

where n_{eff} is the effective refractive index of the fiber and Λ is the grating period. When the FBG is subjected to external effects such as mechanical strain or temperature variations, changes in n_{eff} or Λ lead to a shift in the Bragg wavelength. When an FBG is subjected to mechanical strain and temperature variation, the Bragg wavelength shift is affected by both effects simultaneously. Therefore, under real operating conditions, the measured wavelength shift cannot be directly attributed to strain or temperature alone.[10] The relationship among temperature, strain, and the reflected Bragg wavelength can be expressed as

$$\Delta\lambda_B = \lambda_B\left[\left(1-p_e\right)\cdot\varepsilon + (\alpha+\xi)\cdot\Delta T\right], \tag{2}$$

where p_e is the effective photoelastic coefficient, ε is the mechanical strain, α is the thermal expansion coefficient, ξ is the thermo-optic coefficient, and ΔT is the temperature change. When

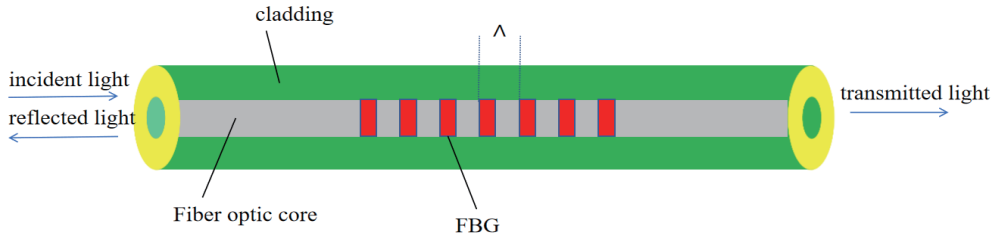

Fig. 1. (Color online) Scheme of the structure of a FBG sensor.

both strain and temperature act on the FBG, defining $K_\varepsilon = \lambda_B \cdot (1 - p_e)$ and $K_T = \lambda_B \cdot (\alpha + \xi)$ leads to the expression

$$\Delta\lambda_B = K_\varepsilon \cdot \varepsilon + K_T \cdot \Delta T\,. \tag{3}$$

In actual wind turbine blade monitoring, strain and temperature vary simultaneously. Therefore, a temperature-compensation FBG is used to measure the local temperature change. For the temperature-compensation FBG, the wavelength shift can be written as

$$\Delta\lambda_T = K_{T,T}\Delta T, \tag{4}$$

where $\Delta\lambda_T$ is the wavelength shift of the temperature-compensation FBG, and $K_{T,T}$ is its temperature sensitivity coefficient. By substituting Eq. (4) into Eq. (3), the mechanical strain can be expressed as

$$\varepsilon = \frac{\Delta\lambda_B - \left(\dfrac{K_T}{K_{T,T}}\right)\Delta\lambda_T}{K_\varepsilon}. \tag{5}$$

Here, K_T and $K_{T,T}$ refer to the temperature sensitivities of the packaged CFRP-FBG strain sensor and the adjacent temperature-compensation FBG, respectively.

2.2 CFRP-FBG packaging and strain transfer process

In this study, the CFRP-FBG sensor is installed on the outer CFRP surface of the wind turbine blade in a surface-bonded configuration. To maximize the strain transfer efficiency from the blade to the FBG, the packaging structure must ensure both material compatibility and adequate interfacial bonding performance. The sensor assembly consists of the following four main components:

(i) FBG sensing element (a bare FBG with its coating removed to enhance strain measurement accuracy),
(ii) CFRP encapsulation layer (a small plate made from unidirectional carbon-fiber prepreg cured into shape, serving as both the substrate and protective layer for the FBG),
(iii) adhesive layer (an epoxy resin compatible with the blade material, bonding the packaged sensor to the blade surface), and
(iv) CFRP surface of the wind turbine blade.

As shown in Fig. 2, Fig. 2(a) presents the overall view of the CFRP-FBG sensor, while Fig. 2(b) shows the cross-sectional view of the sensor bonded to the blade surface. The sensor consists of an optical fiber containing the FBG sensing region, a CFRP encapsulation layer, a bonding layer, and the blade surface. During operation, the surface strain of the wind turbine blade is transferred through the bonding layer and the CFRP encapsulation layer to the embedded FBG sensing region.

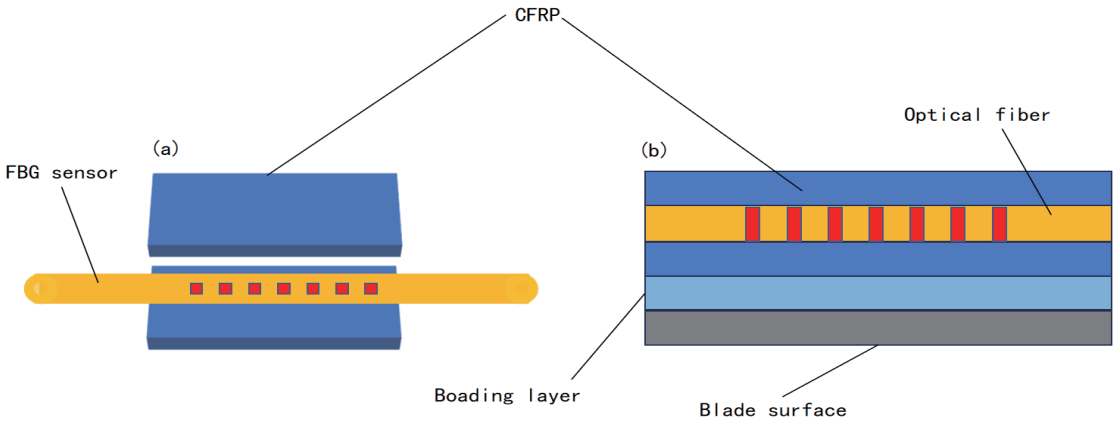

Fig. 2. (Color online) Structural model of the CFRP-FBG sensor: (a) overall view of the CFRP-FBG sensor; (b) cross-sectional view of the sensor bonded to the blade surface.

During operation, aerodynamic loads cause bending deformation of the wind turbine blade, and the resulting surface axial strain is transferred through the adhesive layer and the CFRP encapsulation layer to the embedded FBG. Because the CFRP encapsulation layer has the same material composition and fiber orientation as the blade substrate, it reduces interfacial mismatch and improves strain transfer efficiency. With appropriate encapsulation dimensions and adhesive thickness, the FBG can be mechanically protected while maintaining efficient strain transfer.

When the blade is subjected to aerodynamic loads, local deformation is generated and transmitted to the CFRP layer, inducing strain in the CFRP material. Because the FBG is firmly bonded to the CFRP, this strain is transferred to the fiber core, causing a change in the grating period and a corresponding shift in the reflected Bragg wavelength. By measuring this wavelength shift, the structural strain can be determined. The strain transfer efficiency is defined as the ratio of the strain measured by the FBG to the actual structural strain. Let L be the bonding length, and assume that the material properties and geometric dimensions of each layer are known. The stress distribution within the layered structure is illustrated in Fig. 3(a), while the displacement fields and interfacial relative slips are shown in Fig. 3(b). Here, σ denotes axial stress, τ denotes shear stress, and the subscripts f, c, a, and s refer to variables associated with the FBG, CFRP layer, adhesive layer, and blade surface, respectively; u represents the displacement of each layer. By taking a differential element dx along the x-axis for the substrate-based FBG strain sensor, characteristic analysis is performed for each layer.[11,12] The resulting expression for the average strain transfer is

$$\beta(\mathrm{x}) = 1 - \frac{\sinh(kL)}{kL\cos(kL)^{\omega}}, \tag{6}$$

where k is the strain lag coefficient. According to Eq. (6), as the bonding length increases, the strain transfer efficiency also increases. Therefore, selecting an appropriate length for the

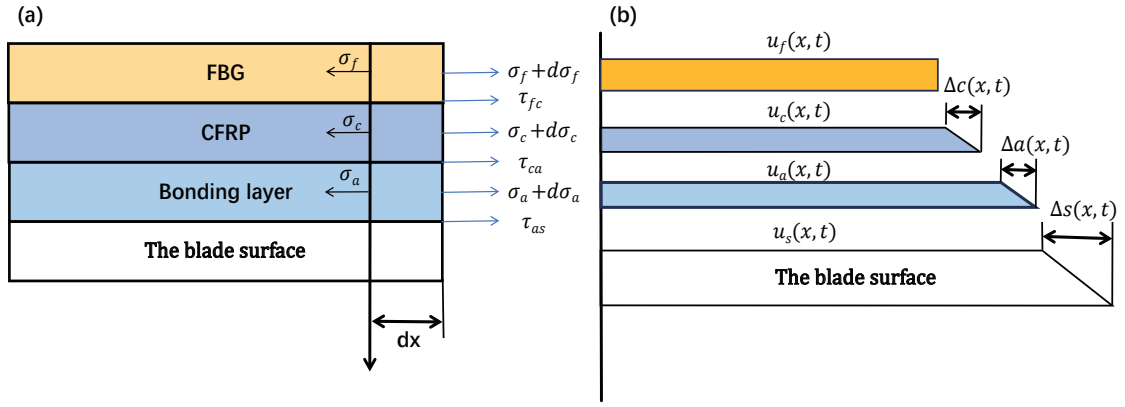

Fig. 3. (Color online) (a) Stress distribution in the layered structure and (b) displacement fields and interfacial relative slip of each layer.

encapsulation layer is crucial. Considering various safety and practical constraints, a final encapsulation length of 100 mm and a width of 10 mm is adopted. It is essential to use encapsulation plates of the correct length during fabrication, as this parameter has a significant influence on strain transfer efficiency.[13]

In this study, the Bragg wavelength of the CFRP-FBG sensor was acquired and demodulated using an FT16 FBG interrogator manufactured by Beijing Dacheng Yongsheng. The interrogator has a wavelength range of 1525–1565 nm and a demodulation resolution of 1 pm. The block diagram of the FBG interrogation system is shown in Fig. 4.

3. Experimental Testing

3.1 Static strain calibration results

Three fabricated CFRP-FBG sensors and one metallic resistance strain gauge were selected for comparison. All static calibration tests were conducted at 23 °C. A steel cantilever beam was used, with an effective cantilever length of 110.5 mm, a width of 40 mm, a thickness of 9.5 mm, and a Young's modulus of 2.0×10^{11} Pa. All sensors were mounted on the same surface of the cantilever beam within the same effective measurement region, so that they were subjected to the same surface strain under static loading.

Applied masses of 3, 6, 9, 12, and 15 kg were successively suspended at the free end of the beam, corresponding to equivalent end forces of 29.43, 58.86, 88.29, 117.72, and 147.15 N, respectively, according to $W = mg$ (g = 9.81 m/s^2). Each load level was maintained for approximately 1 min to record stabilized readings from the FBG interrogator and the strain gauge. The beam was then unloaded stepwise to complete one loading–unloading cycle. This procedure was repeated three times to evaluate sensor linearity, repeatability, and hysteresis. According to Euler–Bernoulli beam theory, the theoretical surface strain can be expressed as

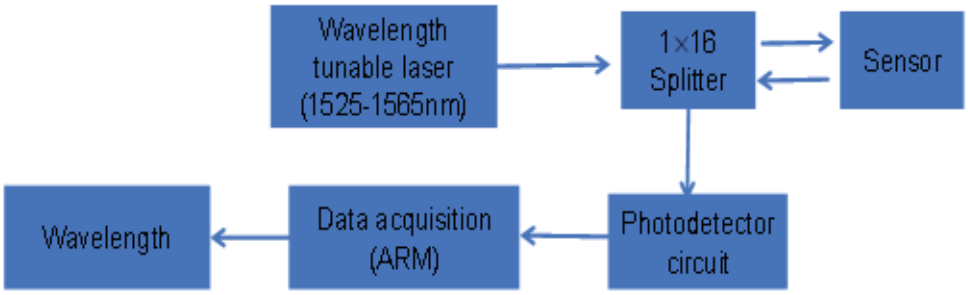

Fig. 4. (Color online) Block diagram of the FBG interrogation system.

$$\varepsilon = \frac{6WL}{Ebh^2}, \tag{7}$$

where ε is the theoretical surface strain, W is the applied end force, L is the effective cantilever length, E is the Young's modulus of the beam material, b is the beam width, and h is the beam thickness. Using the above equation, the theoretical strain values under the five loading levels were calculated.

Figure 5 shows the wavelength–strain relationship of the CFRP-FBG sensor during the static loading–unloading tests on the cantilever beam. The horizontal axis represents the axial surface strain of the beam measured by the electrical strain gauge, while the vertical axis represents the wavelength shift of the FBG. The blue squares correspond to the loading process, and the orange triangles correspond to the unloading process. It can be observed that the reflected wavelength increases almost linearly with strain, and the loading and unloading data nearly overlap, indicating no obvious hysteresis. These results indicate that the sensor exhibits good linearity and negligible hysteresis within the tested strain range. The representative wavelength–strain data corresponding to the loading and unloading processes shown in Fig. 5 are summarized in Table 1.

The loading and unloading experiments were repeated three times. The fitted curves of the Bragg wavelength shift versus strain are shown in Fig. 6, where Fig. 6(a) presents the results of the three loading tests and Fig. 6(b) presents those of the three unloading tests. The three sets of curves remain within a highly linear range. By averaging the results of the three tests, the strain sensitivity of the CFRP-FBG sensor was determined to be 1.22 pm/με, with a linear fitting coefficient of 0.9998. The fitted sensitivities and fitting coefficients of the three repeated loading and unloading experiments are summarized in Table 2.

The theoretical strain, the CFRP-FBG measurements, and the electrical strain-gauge measurements under the five static loading levels are compared in Fig. 7. The experimental results exhibit excellent consistency, with deviations between the experimental values and the strain-gauge measurements within 2%, and deviations between the experimental and theoretical

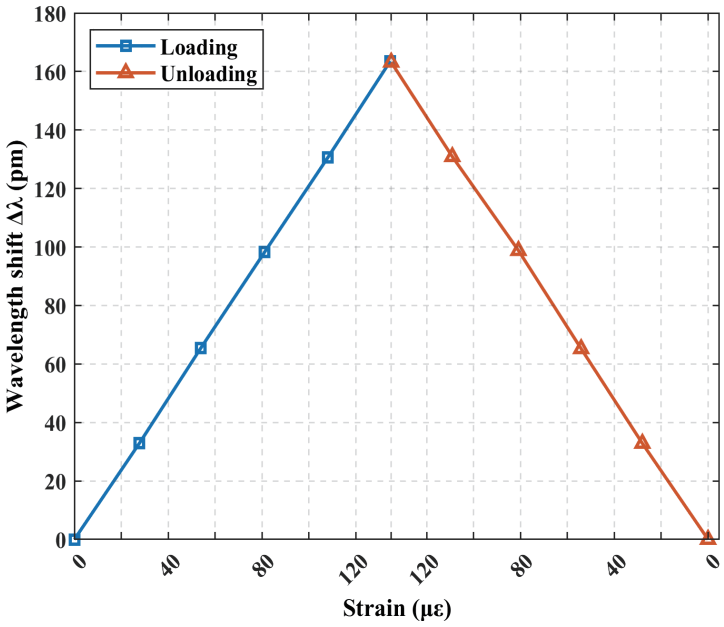

Fig. 5. (Color online) Wavelength–strain relationship of the CFRP-FBG sensor during static loading–unloading tests.

Table 1
Representative wavelength–strain data of the CFRP-FBG sensor.

Process	Level	Strain (με)	Wavelength shift Δλ (pm)
Loading	1	27.81	32.969
Loading	2	53.97	65.467
Loading	3	81.15	98.255
Loading	4	108.12	130.584
Loading	5	134.78	163.566
Unloading	1	135.15	163.18
Unloading	2	109.08	130.88
Unloading	3	80.87	98.79
Unloading	4	54.13	65.21
Unloading	5	28.01	32.83

values within 1%. These results verify the high accuracy of the CFRP-FBG sensor for strain measurement. In other words, the strain transfer efficiency of the CFRP-FBG sensor reaches over 98%, closely approaching ideal behavior. This clearly demonstrates the feasibility and effectiveness of using CFRP-FBG sensors for wind turbine blade strain monitoring.

It is worth noting that traditional resistance strain gauges often experience sensitivity drift and zero-point shift after multiple loading cycles, whereas the FBG sensor maintained highly consistent output after three repeated cycles in this experiment, demonstrating superior stability.

For an FBG with a center wavelength of approximately 1550 nm, the typical strain sensitivity is about 1.0–1.2 pm/με. In this study, the measured sensitivity of the CFRP-FBG sensor is

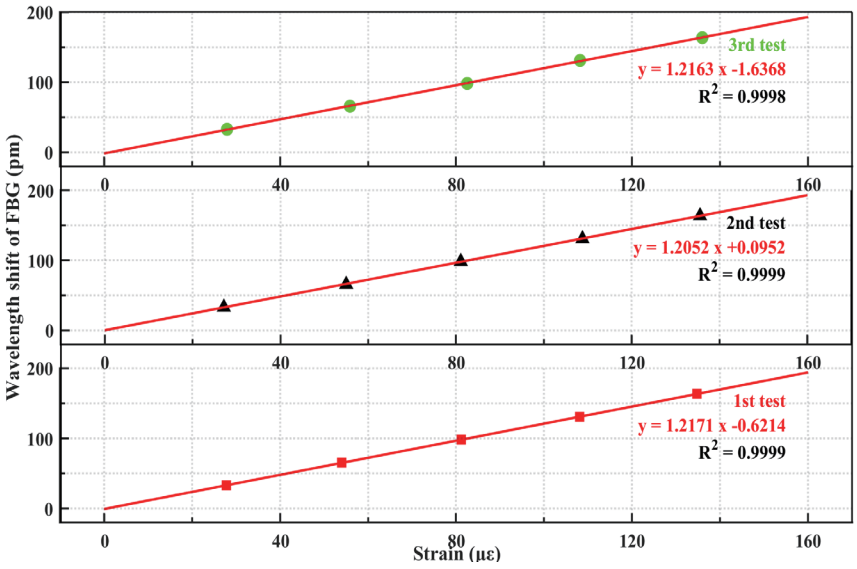

(a)

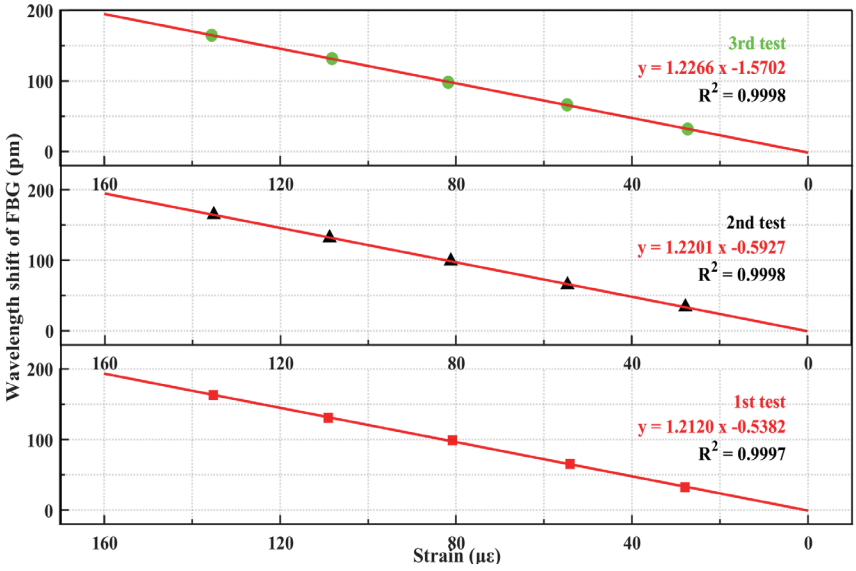

(b)

Fig. 6. (Color online) Fitting results of the three repeated experiments: (a) loading tests; (b) unloading tests.

Table 2
Summary of the fitting results of the three repeated experiments used for Fig. 6.

Test No.	Loading sensitivity (pm/με)	Loading adjusted R^2	Unloading sensitivity (pm/με)	Unloading adjusted R^2
1	1.2171	0.99995	1.2120	0.99966
2	1.2052	0.99988	1.2201	0.99981
3	1.2163	0.99974	1.2266	0.99985
Average	1.2129	0.99986	1.2196	0.99977

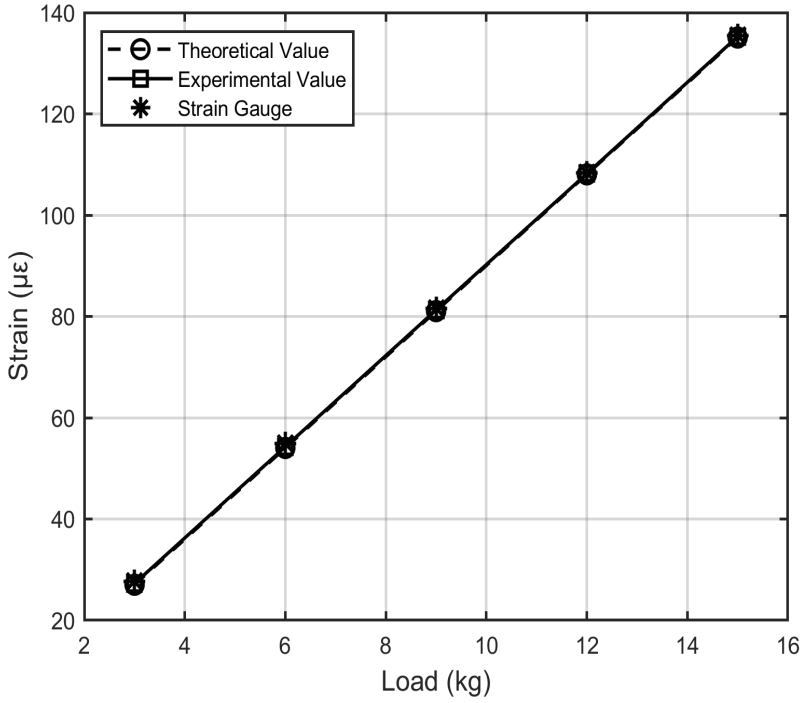

Fig. 7. Theoretical strain, electrical strain-gauge measurements, and CFRP-FBG measurements under five static loading levels.

approximately 1.22 pm/με, which aligns closely with the theoretical value, indicating that the packaging process has almost no effect on the intrinsic strain response of the grating. On the basis of this sensitivity, a static strain of 100 με produces a wavelength shift of about 120 pm, which is significantly larger than the typical demodulation resolution of 1 pm (or even higher) offered by standard interrogators. Therefore, even within the engineering-relevant small-strain range investigated in this study, small strain variations can be clearly and reliably captured. In other words, the strain range selected in this study not only covers the representative strain levels encountered during blade operation but also fully demonstrates the advantages of the CFRP-FBG sensor in terms of small-strain resolution and strain transfer efficiency.

It should be noted that the sensing characteristics and practical applicability of bare FBG have been extensively reported in previous studies.[14,15] Building upon this foundation, the present work is focused on determining whether the CFRP packaging structure alters the sensitivity or linearity of the FBG within the actual service strain range of wind turbine blades, and whether it can maintain high signal-to-noise ratio and repeatability in the small-strain range relevant to engineering applications. The static calibration results show that the strain sensitivity of the CFRP-FBG sensor is essentially consistent with the theoretical value, with excellent linearity in the fitted curves, and the loading–unloading cycles overlap closely, indirectly confirming the strain transfer efficiency and measurement stability of the packaging structure.

3.2 Temperature experiment results

For temperature calibration, the packaged CFRP-FBG sensor specimen, rather than the cantilever-beam assembly, was placed in a temperature-controlled chamber under minimal external mechanical constraint. The temperature was increased from −60 to 60 °C in steps of 20 °C, with each temperature level held for approximately 30 min to allow the wavelength to stabilize before recording the reflected Bragg wavelength. By plotting temperature on the horizontal axis and wavelength (or wavelength shift) on the vertical axis and performing linear fitting, the temperature sensitivity coefficient and linear correlation coefficient of the sensor were obtained, as shown in Fig. 8.

The temperature sensitivity was determined to be 18.6307 pm/K, and the total wavelength shift of the FBG reached approximately 2.23 nm, indicating a strong linear temperature response. Within the tested temperature range from −60 to 60 °C, the packaged CFRP-FBG sensor exhibited stable and nearly linear wavelength variation without abnormal signal fluctuation or loss. The calibrated temperature sensitivity is slightly higher than that of a bare FBG, which is mainly attributed to the thermal expansion effect of the CFRP substrate, imposing an additional influence on the grating and thereby increasing the wavelength drift. It should be noted that the purpose of the present temperature experiment was to calibrate the wavelength–temperature response of the packaged CFRP-FBG sensor under minimal mechanical constraint, rather than to investigate how the strain sensitivity varies with temperature. A systematic study of the temperature dependence of strain sensitivity will be carried out in future work. The

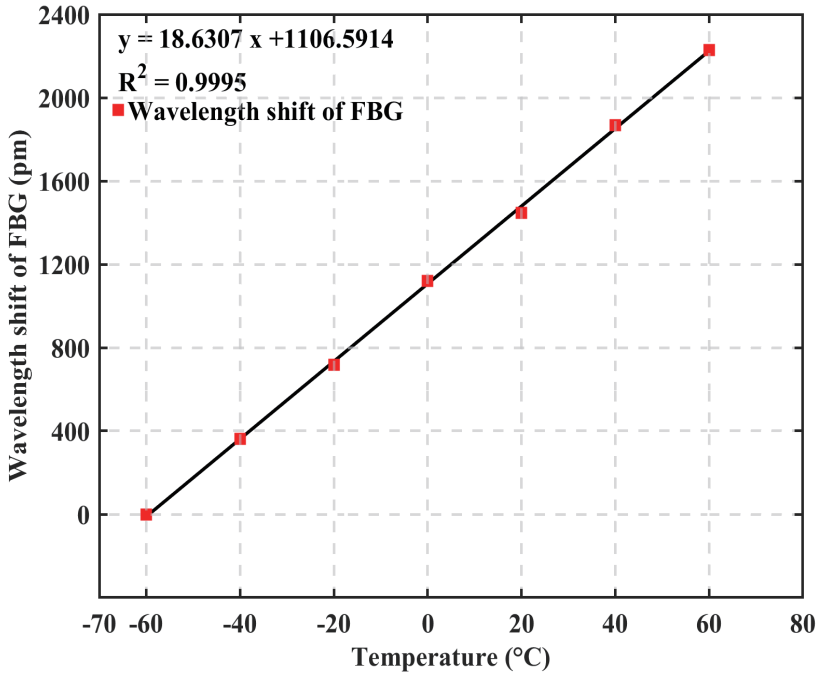

Fig. 8. (Color online) Fitting of results of temperature experiment.

calibrated value of 18.6307 pm/K applies only to the packaged CFRP-FBG sensor specimen and not directly to the temperature-compensation FBGs used in the dynamic test.

4. Dynamic Testing

Four CFRP-FBG strain sensors and four temperature-compensation FBG sensors were installed at four key positions of each blade, such as the leading edge (LE), trailing edge (TE), pressure side (windward side, PS), and suction side (leeward side, SS), with the latter placed adjacent to the strain sensors but positioned to avoid structural loading for temperature compensation. All gratings were routed to the hub center and connected to a high-speed interrogator, with the sampling frequency set to 10 Hz. Figure 9 shows the installation schematic of the sensors. After adhesive bonding and curing for approximately 24 h, the sensors were integrated into the acquisition system, which continuously recorded the wavelength data of each FBG during normal turbine operation and converted them into strain.

In this study, an FS22 interrogator was used to acquire the data. The continuous field monitoring lasted for 72 h. No sensor failure was observed during the monitoring period, and the strain signals remained stable after temperature compensation. Figure 10 shows the strain response of the wind turbine over a 100 s time span. The upper curve (SS) corresponds to the suction side, which undergoes compressive loading, while the lower curve (PS) represents the tensile load on the pressure side. It can be clearly observed that the strain varies repeatedly in a quasi-sinusoidal pattern over time, resulting from the periodic loading applied to the blade during each rotation.

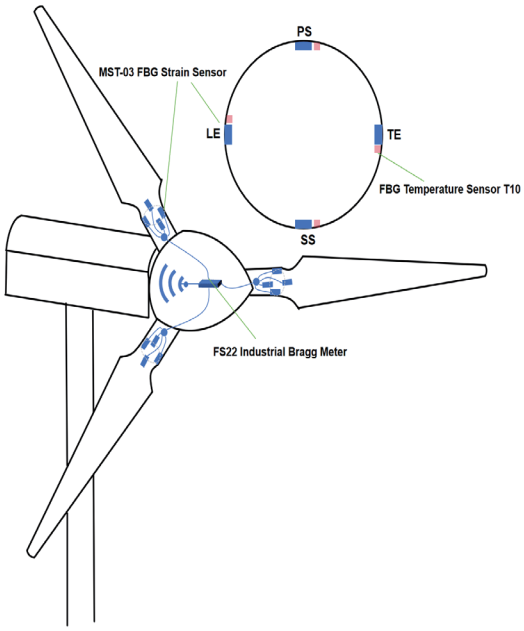

Fig. 9. (Color online) Schematic diagram of sensor installation.

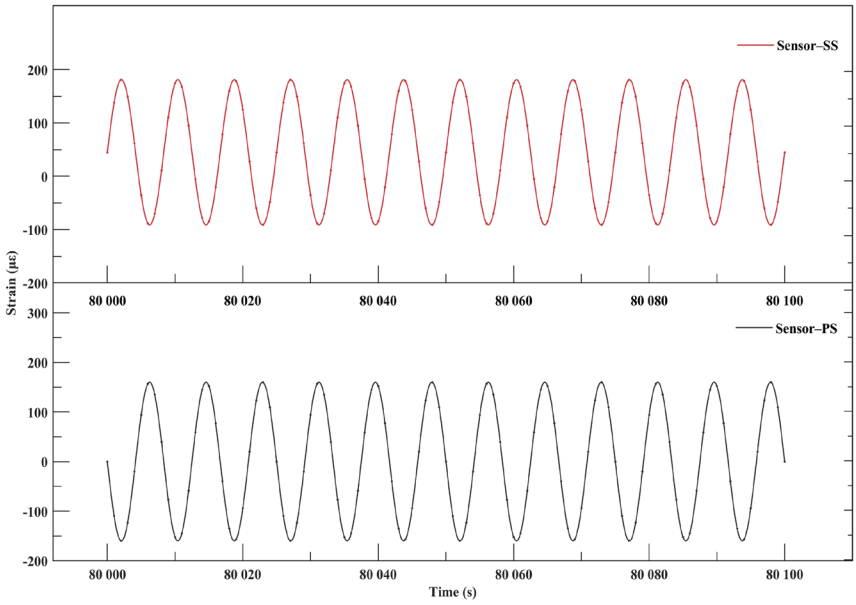

Fig. 10. (Color online) Monitoring results over 100 s.

The strain curves are smooth and continuous, matching the rotational frequency of the blade, demonstrating that the CFRP-FBG sensor can effectively capture the blade's dynamic deformation. Compared with conventional electrical strain gauges reported in the literature, FBG-based sensing is less susceptible to electromagnetic interference and is advantageous for dynamic measurements.[16]

The monitoring results of the CFRP-FBG sensor installed on an actual wind turbine blade demonstrate that the sensor can effectively capture the dynamic strain response of the blade under operating conditions. During the 72 h field monitoring period, no sensor failure or obvious zero drift was observed, and the strain signals remained stable after temperature compensation. The measured strain histories showed smooth and continuous quasi-sinusoidal variations that were consistent with the blade rotational cycle and cyclic loading. These results verify the feasibility of the CFRP-FBG sensor for the online strain monitoring of wind turbine blades under real operating conditions. The present field test mainly demonstrates the dynamic response capability and short-term operational stability of the sensor under real operating conditions. Since structural integrity indicators were not extracted from the transient load data, further long-term investigations are still required to evaluate creep-related effects, long-term drift, and the applicability of the proposed sensor to full structural health monitoring.

5. Conclusions

In this study, a CFRP-FBG surface-bonded sensor was designed and developed for the online monitoring of wind turbine blades. Static cantilever beam loading tests and temperature calibration experiments show that the sensor has a strain sensitivity of approximately 1.22 pm/με

and a linear fitting coefficient of about 0.9998, with deviations from the electrical strain gauge and theoretical values within 2 and 1%, respectively, corresponding to a strain transfer efficiency of over 98%. Within a temperature range of −60 to 60 °C, the sensor exhibits a temperature sensitivity of about 18.63 pm/K and a highly linear wavelength–temperature relationship, demonstrating stable operation across a wide temperature span. When installed at key locations on an operational wind turbine blade—including the leading edge, trailing edge, pressure side, and suction side—the sensor provided dynamic strain measurements that closely matched the blade's rotational speed and loading conditions. No significant zero drift or failure was observed during 72 h of continuous operation, indicating that the CFRP-FBG sensor offers high sensitivity and good continuous monitoring capability under representative operating conditions. It therefore demonstrates feasibility for the online strain and temperature monitoring of wind turbine blades, while further long-term validation of drift behavior and applicability to full structural health monitoring is still required.

Acknowledgments

This work was supported by an industry-commissioned research project funded by Huabei Wind Power Group.

References

1 P. Tchakoua, R. Wamkeue, M. Ouhrouche, F. Slaoui-Hasnaoui, T. A. Tameghe, and G. Ekemb: Energies **7** (2014) 2595. https://doi.org/10.3390/en7042595
2 D. Kinet, P. Mégret, K. W. Goossen, L. Qiu, D. Heider, and C. Caucheteur: Sensors **14** (2014) 7394. https://doi.org/10.3390/s140407394
3 T. J. Arsenault, A. Achuthan, P. Marzocca, C. Grappasonni, and G. Coppotelli: Smart Mater. Struct. **22** (2013) 075027. https://doi.org/10.1088/0964-1726/22/7/075027
4 S. Tian, Z. Yang, X. Chen, and Y. Xie: Sensors **15** (2015) 19992. https://doi.org/10.3390/s150819992
5 B. Wen, X. Tian, Z. Jiang, Z. Li, X. Dong, and Z. Peng: Mar. Struct. **71** (2020) 102729. https://doi.org/10.1016/j.marstruc.2020.102729
6 G. F. Pereira: Multi-life-stage monitoring system based on fibre bragg grating sensors for more reliable wind turbine rotor blades: Experimental and numerical analysis of deformation and failure in composite materials, Ph.D. thesis, DTU Wind Energy, Technical University of Denmark, Kgs. Lyngby (2016). https://orbit.dtu.dk/en/publications/multi-life-stage-monitoring-system-based-on-fibre-bragg-grating-s
7 D. Li, S. C. M. Ho, and G. Song: Smart Mater. Struct. **24** (2015) 033001. https://doi.org/10.1088/0964-1726/24/3/033001
8 W. Wang, Y. Xue, C. He, and Y. Zhao: Energies **15** (2022) 5672. https://doi.org/10.3390/en15155672
9 P. Zhu, X. Feng, Z. Liu, M. Huang, H. Xie, and M. A. Soto: Compos. Sci. Technol. **213** (2021) 108933. https://doi.org/10.1016/j.compscitech.2021.108933
10 X. Shu, Y. Liu, D. Zhao, B. Gwandu, F. Floreani, L. Zhang, and I. Bennion: Opt. Lett. **27** (2002) 701. https://doi.org/10.1364/OL.27.000701
11 M. Liang, N. Chen, X. Fang, and G. Wu: Appl. Opt. **57** (2018) 5837. https://doi.org/10.1364/AO.57.005837
12 L. Sun, C. Li, C. Zhang, T. Liang, and Z. Zhao: Sensors **19** (2019) 1851. https://doi.org/10.3390/s19081851
13 G. Xue, X. Fang, X. Hu, and L. Gong: Appl. Opt. **57** (2018) 2939. https://doi.org/10.1364/AO.57.002939
14 G. Allwood, G. Wild, and S. Hinckley: Electronics **6** (2017) 92. https://doi.org/10.3390/electronics6040092
15 J. K. Sahota, N. Gupta, and D. Dhawan: Opt. Eng. **59** (2020) 060901. https://doi.org/10.1117/1.OE.59.6.060901
16 G. Szebényi, Y. Blößl, G. Hegedűs, T. Tábi, T. Czigány, and R. Schledjewski: Compos. Sci. Technol. **199** (2020) 108317. https://doi.org/10.1016/j.compscitech.2020.108317